

# Robust microfiber photonic microcells for sensor and device applications

Wa Jin,<sup>1,2</sup> Haifeng Xuan,<sup>1</sup> Chao Wang,<sup>1,2</sup> Wei Jin,<sup>1,2,\*</sup> and Yiping Wang<sup>3</sup>

<sup>1</sup>Department of Electrical Engineering, The Hong Kong Polytechnic University, Hong Kong, China

<sup>2</sup>The Hong Kong Polytechnic University Shenzhen Research Institute, Shenzhen, China

<sup>3</sup>College of Optoelectronic Engineering, Shenzhen University, Shenzhen, China

[eewjin@polyu.edu.hk](mailto:eewjin@polyu.edu.hk)

**Abstract:** We report the fabrication of in-line photonic microcells (PMCs) by encapsulating tapered microfibers (MFs) inside glass tubes. The encapsulation isolates MFs from external environment and makes them more suitable for real-world applications. Based on PMCs with encapsulated highly birefringent (Hi-Bi) MFs, we demonstrated pressure, temperature and refractive index (RI) sensors as well as long period grating devices. A fiber Sagnac loop interferometer incorporating a Hi-Bi microfiber PMC demonstrated RI sensitivity of 2024 nm per RI unit (nm/RIU) in gaseous environment and 21231 nm/RIU in water.

©2014 Optical Society of America

**OCIS codes:** (060.2310) Fiber optics; (060.2370) Fiber optics sensors; (060.2340) Fiber optics components; (230.3990) Micro-optical devices; (060.2420) Fibers, polarization-maintaining; (060.4005) Microstructured fibers.

---

## References and links

1. X. S. Jiang, Y. Chen, G. Vienne, and L. M. Tong, "All-fiber add-drop filters based on microfiber knot resonators," *Opt. Lett.* **32**(12), 1710–1712 (2007).
2. M. Sumetsky, "Basic elements for microfiber photonics: Micro/nanofibers and microfiber coil resonators," *J. Lightwave Technol.* **26**(1), 21–27 (2008).
3. P. Pal and W. H. Knox, "Fabrication and characterization of fused microfiber resonators," *IEEE Photon. Technol. Lett.* **21**(12), 766–768 (2009).
4. S. Leon-Saval, T. Birks, W. Wadsworth, P. St. J. Russell, and M. Mason, "Supercontinuum generation in submicron fibre waveguides," *Opt. Express* **12**(13), 2864–2869 (2004).
5. G. Salceda-Delgado, D. Monzon-Hernandez, A. Martinez-Rios, G. A. Cardenas-Sevilla, and J. Villatoro, "Optical microfiber mode interferometer for temperature-independent refractometric sensing," *Opt. Lett.* **37**(11), 1974–1976 (2012).
6. Y. Cao, W. Jin, L. H. Ho, and Z. Liu, "Evanescent-wave photoacoustic spectroscopy with optical micro/nano fibers," *Opt. Lett.* **37**(2), 214–216 (2012).
7. L. Xiao, M. D. W. Grogan, W. J. Wadsworth, R. England, and T. A. Birks, "Stable low-loss optical nanofibres embedded in hydrophobic aerogel," *Opt. Express* **19**(2), 764–769 (2011).
8. F. Xu and G. Brambilla, "Preservation of micro-optical fibers by embedding," *Jpn. J. Appl. Phys.* **47**(8), 6675–6677 (2008).
9. T. A. Birks, W. J. Wadsworth, and P. S. Russell, "Supercontinuum generation in tapered fibers," *Opt. Lett.* **25**(19), 1415–1417 (2000).
10. F. Xu and G. Brambilla, "Preservation of micro-optical fibers by embedding," *Jpn. J. Appl. Phys.* **47**(8), 6675–6677 (2008).
11. N. Lou, R. Jha, J. L. Domínguez-Juárez, V. Finazzi, J. Villatoro, G. Badenes, and V. Pruneri, "Embedded optical micro/nano-fibers for stable devices," *Opt. Lett.* **35**(4), 571–573 (2010).
12. G. Vienne, Y. Li, and L. M. Tong, "Effect of host polymer on microfiber resonator," *IEEE Photon. Technol. Lett.* **19**(18), 1386–1388 (2007).
13. L. M. Xiao, M. D. W. Grogan, W. J. Wadsworth, R. England, and T. A. Birks, "Stable low-loss optical nanofibres embedded in hydrophobic aerogel," *Opt. Express* **19**(2), 764–769 (2011).
14. H. Xuan, J. Ju, and W. Jin, "Highly birefringent optical microfibers," *Opt. Express* **18**(4), 3828–3839 (2010).
15. W. Jin, C. Wang, H. Xuan, and W. Jin, "Tunable comb filters and refractive index sensors based on fiber loop mirror with inline high birefringence microfiber," *Opt. Lett.* **38**(21), 4277–4280 (2013).
16. S. Geacai, I. Nita, O. Iulian, and E. Geacai, "Refractive indices for biodiesel mixtures," *U. P. B. Sci. Bull. Series B* **74**(4), 149–160 (2012).
17. D.-W. Duan, Y.-J. Rao, and T. Zhu, "High sensitivity gas refractometer based on all-fiber open-cavity Fabry-

- Perot interferometer formed by large lateral offset splicing,” *J. Opt. Soc. Am. B* **29**(5), 912–915 (2012).
18. Z. Liu, C. Wu, M.-L. V. Tse, C. Lu, and H.-Y. Tam, “Ultrahigh birefringence index-guiding photonic crystal fiber and its application for pressure and temperature discrimination,” *Opt. Lett.* **38**(9), 1385–1387 (2013).
  19. W. Jin, H.-F. Xuan, C. Wang, and W. Jin, “High sensitivity pressure sensor based on a birefringent microfiber loop mirror,” *Proc. SPIE* **8924**, 89242Z (2013).
  20. P. Schiebener, J. Straub, J. M. H. Levelt Sengers, and J. S. Gallagher, “Refractive index of water and steam as function of wavelength, temperature and density,” *J. Phys. Chem. Ref. Data* **19**(3), 677–717 (1990).
  21. J. Li, L.-P. Sun, S. Gao, Z. Quan, Y.-L. Chang, Y. Ran, L. Jin, and B.-O. Guan, “Ultrasensitive refractive-index sensors based on rectangular silica microfibers,” *Opt. Lett.* **36**(18), 3593–3595 (2011).
  22. H. Xuan, W. Jin, and S. Liu, “Long-period gratings in wavelength-scale microfibers,” *Opt. Lett.* **35**(1), 85–87 (2010).
  23. H. Xuan, W. Jin, and M. Zhang, “CO<sub>2</sub> laser induced long period gratings in optical microfibers,” *Opt. Express* **17**(24), 21882–21890 (2009).
- 

## 1. Introduction

Microfiber (MF) photonic devices have attracted considerable attention recently. Various MF-based devices such as microfiber resonators and add/drop filters [1–3], supercontinuum sources [4], refractometric sensors, and photoacoustic gas detectors [5,6] have been reported. Many of these devices take advantage of the large external evanescent field of MFs and exploit the strong interaction between the evanescent field and surrounding media, which form the basis for a range of chemical, biological and environmental sensors. However, the optical performance of the MFs degrades quickly due to light scattering from dust particles and cracks induced by water vapor, and an increasing unrecoverable optical loss was observed over time if they are left in open air [7,8]. Moreover, the MFs are fragile and not easy to handle, which hinders practical applications of these fibers.

In this paper, we report the fabrication of photonic microcells (PMCs) by encapsulating a MF within a glass capillary. The MFs are fabricated by bi-tapering a conventional single mode fiber (SMF) and suspended along the center line of a capillary tube. The MF is kept straight within the capillary tube while its SMF pigtauls are glued to the two ends of the capillary. The encapsulation does not change the optical property of the MF but the capillary tube protects the MF from external disturbance and contamination and makes it more robust. Side holes are made on the capillary wall, which act as ingress/egress channels for sample liquids or gases. Such PMCs are robust and stable, and can be easily integrated into standard fiber-optic circuits with low loss, making the MF-based devices more practical for real-world applications. To illustrate the potential applications of such PMCs, we demonstrated refractive index (RI) sensors by incorporating an encapsulated highly birefringent (Hi-Bi) microfiber PMC into a fiber-optic Sagnac loop interferometer (SLI) and achieved RI sensitivity of 2024 nm per RI unit (RIU) around RI = 1 and 21231 nm/RIU around RI = 1.33. We also demonstrated the fabrication of long period gratings (LPGs) by scanning a focused femtosecond infrared laser beam directly across an encapsulated Hi-Bi microfiber, and by scanning a pulsed CO<sub>2</sub> laser beam across a non-encapsulated Hi-Bi MF and encapsulating the MF after the LPG is fabricated on it.

## 2. 2. Fabrication of encapsulated MF PMCs

The setup for fabricating encapsulated MF PMCs is schematically shown in Fig. 1. It is a home-made tapering-rig based on the well-known flame-brushing technique, and this technique is popularly used to taper-draw MFs from conventional SMFs [9]. An additional three-axis translation stage with a tube holder was used to support a capillary tube within which the MF is going to be housed. The SMF is firstly inserted into the capillary mounted on the tube holder and the SMF tails on the two sides of the capillary are clamped on two fiber holders on the tapering rig. Before tapering, the position of the capillary is adjusted carefully to ensure the SMF is located approximately along the central axis of the capillary tube. The capillary is initially moved away from the central flame-brushing region so that the MF taper could be made by the standard taper-draw process. After the tapering process is completed,

the capillary is carefully moved back to cover the tapered region. The length of the capillary is selected to be longer than the tapered region so that the two ends of the capillary could be glued to the SMF pigtails without disturbing the MF section.

The capillary used in our experiment has inner and outer diameters of  $\sim 660 \mu\text{m}$  and  $\sim 900 \mu\text{m}$ , respectively. To ensure the MF is suspended along the central axis of the capillary, two shorter capillaries ( $\sim 3 \text{ mm}$  in length) with inner and outer diameters of  $\sim 320 \mu\text{m}$  and  $500 \mu\text{m}$  are inserted into the two ends of the larger capillary and they are fixed together by glue. The SMF and the capillary assembly are then glued together and the MF is then encapsulated inside the capillary tube. Figure 2 shows a sketch, the photo and microscope images of a typical PMC. The detail of the MF inside the capillary is shown in Fig. 2(e), and the MF is straight and suspended along the central axis of the capillary tube.

During the process of tapering and encapsulation, the transmission spectrum of the device was monitored by connecting the input and output SMF pigtails respectively to a broadband light source (BLS) and an optical spectrum analyzer (OSA). A large transmission loss was observed if the MF is broken or adhered to the inner wall of the capillary. A loss of  $\sim 0.2 \text{ dB}$  is achieved with a PMC containing a  $5 \text{ cm}$ -long and  $\sim 1 \mu\text{m}$ -diameter MF.

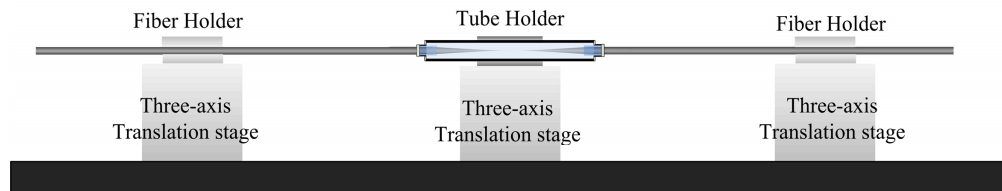


Fig. 1. Setup for encapsulating a microfiber inside a glass capillary.

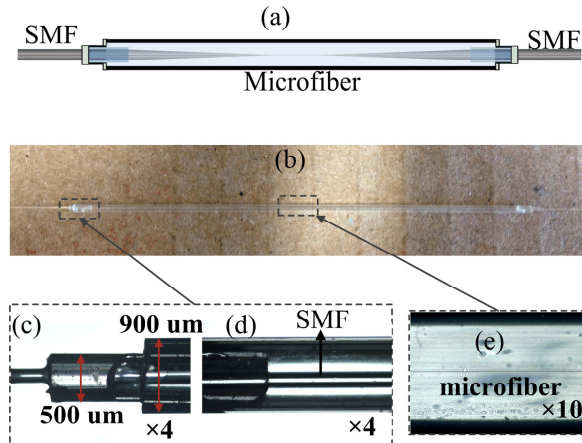


Fig. 2. (a) Schematic and (b) photo of a PMC with an encapsulated MF; (c-e) microscope images of the PMC: (c) the external and (d) the internal of the capillary end, (e) the MF inside the capillary.

There have been researches on protecting MFs by embedding them into various low RI materials such as Teflon [10,11] and EFORON PC-373 [12]. The embedment improves robustness, stability of the MFs and protects them from environmental degradation. However, it also brought some challenges, including complicated embedding process, additional optical loss [10,11], undesirable changes in light confinement and dispersion [10,12], and incapability of accessing to the evanescent field. With the porous silica aerogel coating [13], the access of evanescent field by gas species is still possible, however, it would be difficult for the liquid samples. The brittleness of the aerogel would also limit the practical applications of such devices. The PMCs described above overcomes the aforementioned

limitations, the encapsulation does not change the optical properties of the MF but provide a miniature container for sample liquids or gases, avoiding the use of bulky gas or liquid chambers. However, it should be pointed out that the PMCs are suitable for straight MFs and MF-based devices and they cannot be used to house MF knots and loops [1, 3].

### 3. Encapsulated Hi-Bi MF PMCs and sensors

With the above described technique, we made PMCs with a Hi-Bi MF encapsulated inside a silica capillary tube. The Hi-Bi MF was taper-drawn from a commercial SMF-28 fiber. The fiber was firstly “cut” by use of a femtosecond IR laser to remove parts of the cladding on both sides of the fiber, and the cut region was then tapered down to a MF with an approximately elliptical shape. The detailed process for fabricating Hi-Bi MF tapers has been described in previous papers [14,15]. The Hi-Bi MF was then encapsulated inside a silica capillary. Before the start of tapering, the cut SMF was spliced into a Sagnac loop interferometer (SLI) [15] and the evolution of loss and birefringence of the MF were monitored continuously by observing the transmission spectrum of the interferometer.

Figure 3 shows the output spectrums of a SLI incorporating an encapsulated elliptical MF with a uniform waist region of  $\sim 1$  cm, an ellipticity of 0.7, and a major diameter of  $\sim 2.8 \mu m$ . The MF was encapsulated inside a silica capillary with inner diameter of  $\sim 900 \mu m$  and two side-holes with diameter of  $\sim 400 \mu m$  were made near the two ends of the capillary. As can be seen from Fig. 3(a), no variation in the transmission spectrum was observed before and after encapsulation. The spectrums of the encapsulated and non-encapsulated Hi-Bi MF at different times are shown in Fig. 3(b). The effectiveness of encapsulation on the long term stability of the MF is obvious.

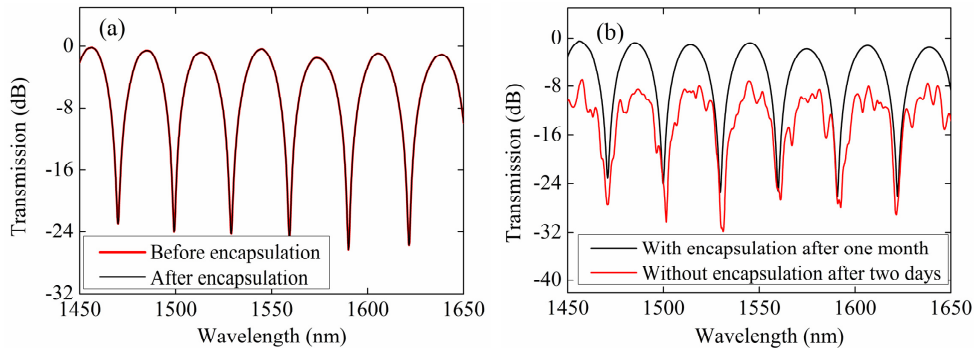


Fig. 3. Spectrums of output light from a SLI containing a Hi-Bi MF. (a) Spectrums before and after encapsulation. (b) Spectrums of encapsulated Hi-Bi MF after one month and non-encapsulated MF left open in air for two days.

#### 3.1 Gas pressure and RI sensors

Before performing pressure and RI measurements, the influence of temperature on the transmission spectrum was firstly studied. By placing the encapsulated Hi-Bi MF PMC into a digitally controlled oven, the output spectrum of the SLI was recorded when the temperature was varied from 25 to 100 °C in steps of 25 °C. Two 400  $\mu m$ -diameter holes were made on the PMC's capillary wall and kept open to ambient environment so that the pressure inside the capillary is maintained at atmospheric pressure. Figure 4(a) shows the spectrums at 25 and 100 °C, and the wavelength of the dip around 1558 nm as function of temperature is shown in Fig. 4(b). The temperature slope is small and  $\sim 7.7 \text{ pm}/\text{°C}$ , which is similar to that a non-encapsulated Hi-Bi MF and is believed due mainly to the thermal-expansion of silica [15].

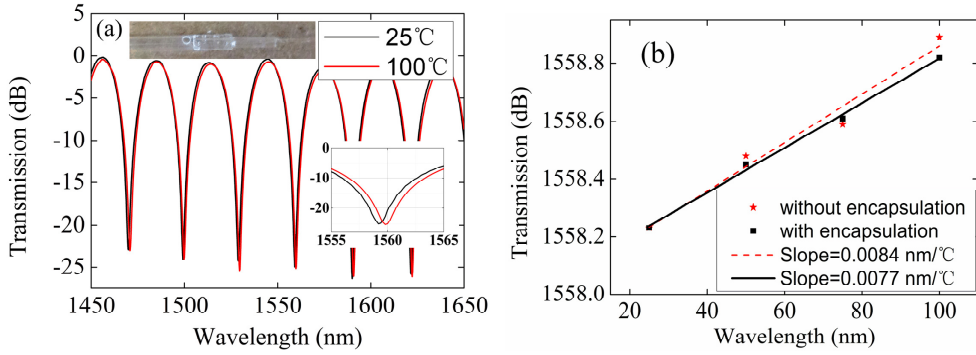


Fig. 4. (a) Output spectrums of a SLI incorporating an encapsulated Hi-Bi microfiber at two different temperatures (25 and 100); (b) Dip wavelength around 1558 nm as a function of temperature for the Hi-Bi MF with (black solid line) and without (red dash line) encapsulation.

The same encapsulated Hi-Bi microfiber sample was then used to measure the RI of a gas mixture. The encapsulated sample was placed inside a gas chamber as shown in Fig. 5(a). The inlet and outlet of the chamber were kept open to make sure that the pressure in the chamber is stable and at atmospheric pressure. Standard hydrogen and nitrogen gases were mixed with different proportions by varying the flow rate of the gases, which were controlled by two digital mass flow controllers (MFCs). The gas mixture was then guided into the gas chamber within which the encapsulated microfiber sample is placed. For a small gas chamber, the gas concentration within the gas chamber and the capillary reaches steady state within seconds, and the RI of the gas mixture may be calculated by using [16]

$$n_m = v_{H_2} n_{H_2} + v_{N_2} n_{N_2} \quad (1)$$

where  $n_m$  is the RI of the gas mixture, and  $n_i$  and  $v_i$  are respectively the refractive indexes and the fraction of the gas component  $i$  ( $i = H_2$  or  $N_2$ ).

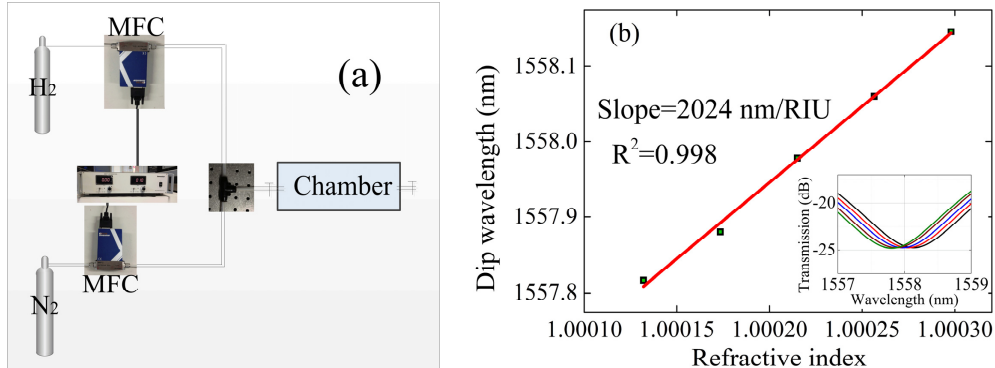


Fig. 5. (a) Setup for producing gas mixtures with different refractive indexes. MFC: mass flow controller. (b) Dip wavelength as a function of refractive index. Inset: spectrums for five different gas mixtures.

The experimental process is as follows: firstly, the hydrogen gas was switched off and the nitrogen gas with a flow rate of 150 sccm (standard cubic centimeter per minute) was continually injected into the chamber, the spectrum was recorded when it became stable, which means that the nitrogen gas had completely filled the chamber. The flow rate of hydrogen gas was then set to 50, 150 and 450 sccm, the evolution of spectrums were recorded. The flow of nitrogen gas was set to 0 sccm and only the hydrogen gas was injected into the chamber, the spectrum was recorded when the chamber was fully filled with

hydrogen. The five recorded spectrums correspond respectively to  $(\nu_i, \nu_i) = (1,0)$ ,  $(3/4, 1/4)$ ,  $(1/2, 1/2)$ ,  $(1/4, 3/4)$  and  $(0,1)$ . Figure 5(b) shows the dip wavelength around 1558 nm as a function of RI of the gas mixture, and the detailed spectrums for the five gas mixtures are shown in the inset of Fig. 5(b). The dip wavelength shifts to the longer wavelength with increasing RI and the slope coefficient or sensitivity is 2024 nm/RIU.

The PMC can also be used as a sensor to measure gas pressure. For the purpose of applying different gas pressure into the capillary tube, one of the two holes on the capillary wall was sealed after the capillary was filled with pure nitrogen and a three port tube as shown in the inset in Fig. 6 was used to change the nitrogen gas pressure inside the capillary. The gas pressure inside the capillary was ramped up or down by a nitrogen gas pump, the experiments were carried out at room temperature ( $\sim 25^\circ\text{C}$ ). The gas pressure change resulted in a change in the RI surrounding the Hi-Bi microfiber, which altered the phase difference between the two orthogonal polarization states. The dip wavelength as a function of gas pressure is shown in Fig. 6, and the pressure sensitivity is 599 pm/bar and is much higher than that of other optical fiber devices [17, 18]. This demonstrates that the PMCs could be used as a miniature gas chamber for gas sensing applications. The PMC with an encapsulated MF in this paper are much more compact and easier to be handled, and more suitable for practical sensing applications than previous one [19].

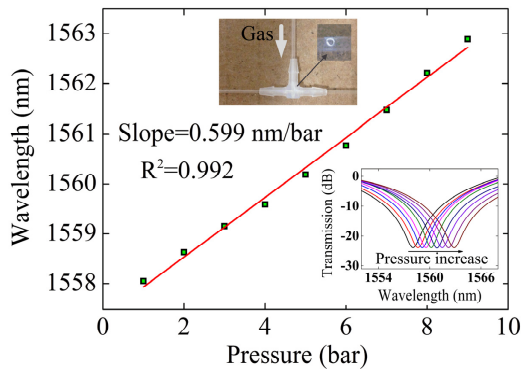


Fig. 6. Dip wavelength around 1558 nm (at room temperature) as a function of gas pressure from 1 to 9 bar.

### 3.2 Liquid refractive index and temperature sensors

The PMC was filled with water to explore its potential application for biosensors. One hole on the capillary wall was immersed into water while the other hole left open to atmosphere, the section between the two side-holes was filled with water in a few second via capillary effect, as shown in the inset Fig. 7(a). The transmission spectrum of the SLI for varying water temperature is shown in Fig. 6. The interference dip around 1548 nm shifted about 70 nm for temperature from 25 to 50  $^\circ\text{C}$ . This shift is due primarily to the thermal-optic coefficient of water RI ( $\sim 1 \times 10^{-4}/^\circ\text{C}$ ) and, as demonstrated in Fig. 3 the temperature sensitivity of the SLI with the microfiber in air is  $\sim 0.008 \text{ nm} / ^\circ\text{C}$  and may be neglected in this experiment. By use of the look-up table in [20], the temperature changes can be converted into RI change and the dip wavelength as function of water RI is plotted in Fig. 7(b). The RI sensitivity is  $\sim 21231 \text{ nm/RIU}$  and similar to that of the non-encapsulated MFs [15]. This shows that the encapsulation does not change the optical properties of MFs but provides a robust and miniature chamber for evanescent field liquid sensing.

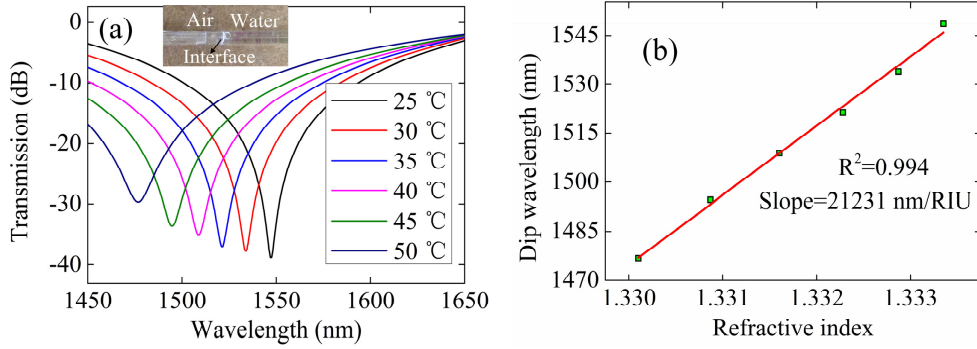


Fig. 7. (a) Measured transmission spectra when temperature is varied from 25 to 50 °C, inset: the region around the hole at the end of the capillarity. (b) Wavelength of the dip around 1548 nm as function of temperature.

The PMC can be cleaned and re-used. By use of a piece of absorbent paper to cover one of the holes on the capillary wall, the majority of water within the microcell can be removed within seconds. The cell was then re-filled with 99.5% propyl alcohol, which was removed by placing the absorbent paper on the hole. This process was repeated for a few times and the microcell left in air for a few minutes to dry out the alcohol. The transmission spectrum of the SLI was found returned to the initial spectrum shown in Fig. 3, indicating that no water was left within the cell. The microcell was then filled with refractive index oil with  $n = 1.3$  and a high thermo-optic coefficient of  $-3.34 \times 10^{-4}/\text{°C}$ . The two side-holes on the capillary were sealed and the transmission spectrums for temperature from 30 to 45°C are shown in Fig. 8(a). The dip wavelength is highly sensitive to temperature with sensitivity of  $-6.99 \text{ nm/}^\circ\text{C}$  as shown in Fig. 8(b).

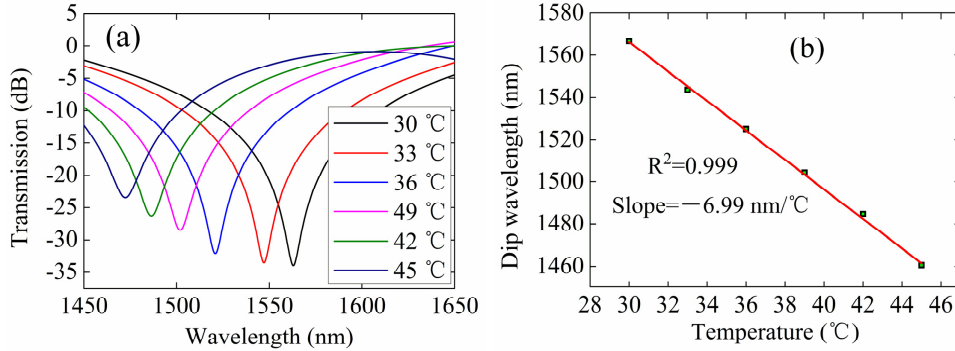


Fig. 8. (a) Measured transmission spectra of the SLI with a Hi-Bi MF microcell filled with RI liquid when temperature is varied from 30 to 40 °C. (b) Dip wavelength as a function of temperature.

### 3.3 Discussion

The sensitivity ( $S$ ) of the dip wavelength ( $\lambda$ ) to RI ( $n$ ) surrounding the Hi-Bi microfiber may be expressed as [21]

$$S = \frac{d\lambda}{dn} = \frac{\lambda \partial B / \partial n}{B - \lambda \partial B / \partial \lambda} = \frac{\lambda \partial B / \partial n}{G} \quad (2)$$

$S$  is determined by the RI induced birefringence variation  $\partial B / \partial n$  and the wavelength-dependent dispersion of birefringence  $\partial B / \partial \lambda$ .  $G$  represents the group birefringence. For

elliptical microfiber used in our experiments,  $b/a = 0.7$  and  $a = 1.4 \mu\text{m}$ , the birefringence  $B$  as function of surrounding RI and the normalized diameter  $\sqrt{2a \times 2b}/\lambda$  is shown in Fig. 9(a). For the RI range shown in Fig. 9(a),  $\partial B/\partial n < 0$ , but the birefringence does not change monotonically with the wavelength. With Eq. (2) and the results in Fig. 9(a), the sensitivity  $S$  was numerically calculated and shown in Fig. 9(b). The experimental results for MF surrounded by air (RI~1) and water (RI~1.33) were also shown in Fig. 9(b), which agree approximately with the numerical results of 2452 nm/RIU and 23165 nm/RIU. Figure 9(b) shows that RI sensitivity may be enhanced significantly when the group birefringence  $G$  approaches zero. However, considering the finite spectrum width of measurement setup (i.e. the OSA), the infinite sensitivity would not be achieved [21].

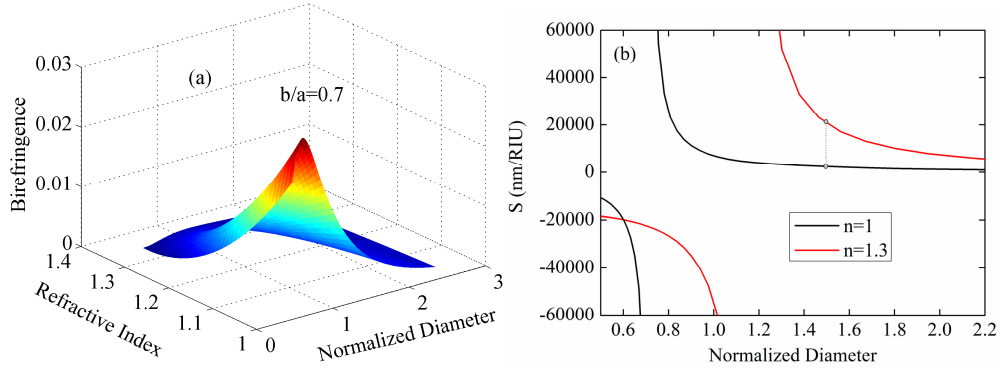


Fig. 9. (a) Calculated Birefringence as a function of normalized diameter. (b) Sensitivity as a function of the fiber width  $a$  at 1550 nm. The experimental results are marked as open circles. Long period grating (LPG) devices.

#### 4.1 Inscription of LPGs with a femtosecond infrared laser

An LPG was fabricated on an encapsulated Hi-Bi MF by scanning a focused femtosecond infrared laser periodically across the PMC. The procedure used is similar to that described in [22] but what we want to show here is that the LPG is made after the encapsulation and, by adjusting the focus and the energy of the femtosecond laser pulses, LPG can be made directly on the MF, regardless of the capillary tube that encapsulates the MF. The encapsulation has little or no effect on the inscription. Figure 10(a) shows a microscope image of the LPG with a period of 20  $\mu\text{m}$ . The laser pulses used had an irradiation intensity of 0.2 J/cm<sup>2</sup> and was focused on the upper surface of Hi-Bi microfiber. The laser exposure time was  $\sim 1$  s. Figure 10(b) shows the transmission spectrum of an LPG made on an encapsulated Hi-Bi microfiber. The MF was made under similar conditions as the one used in section 3 and hence the parameters of the Hi-Bi MF are expected to be similar. The resonance wavelengths for the two orthogonal polarization eigen-states are 1532.7 and 1614.2 nm, and the corresponding grating strengths are 19.2 and 15.2 dB, respectively.

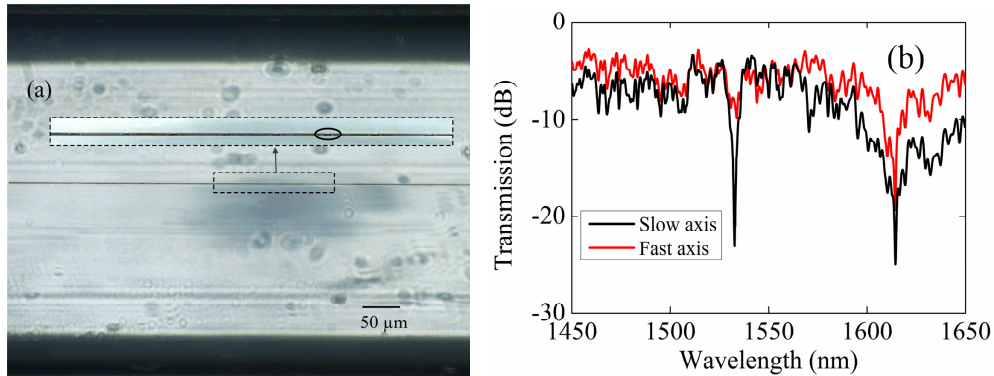


Fig. 10. (a) Microscope image of an LPG showing the periodic notches along the encapsulated Hi-Bi MF. (b) Transmission spectrums of the LPG for two orthogonal polarization eigen states.

#### 4.2 Inscription of LPGs with a CO<sub>2</sub> laser

We also fabricated an LPG in a Hi-Bi MF by use of a low-cost pulsed CO<sub>2</sub> laser to periodically taper the microfiber longitudinally. The LPG was firstly fabricated on the non-encapsulated MF by following a procedure similar to that described in [23], and then the MF with LPG was encapsulated within a capillary tube. The pulse width, repletion rate and average power of CO<sub>2</sub> laser used are respectively to 2.0 μs, 10 kHz and 0.02 W. The CO<sub>2</sub> beam was focused to a spot of ~40 μm in diameter and has a ~50 μm depth of focus. The size of focal spot is considerably larger than the diameter of the MF. Figure 11 shows the transmission spectrums for two orthogonal polarization states immediately after the encapsulation and one month after the encapsulation. The LPG has 25 periods and the pitch of the grating is 150 μm. The resonance wavelengths for the two polarizations are 1445.5 and 1575.6 nm, and the strengths of the attenuation dip are ~12.5 and 20 dB, respectively. The spectrums of the encapsulated LPG showed very little changes over the period of one month and the slight shift of the spectrums could be due to changes in the ambient temperature.

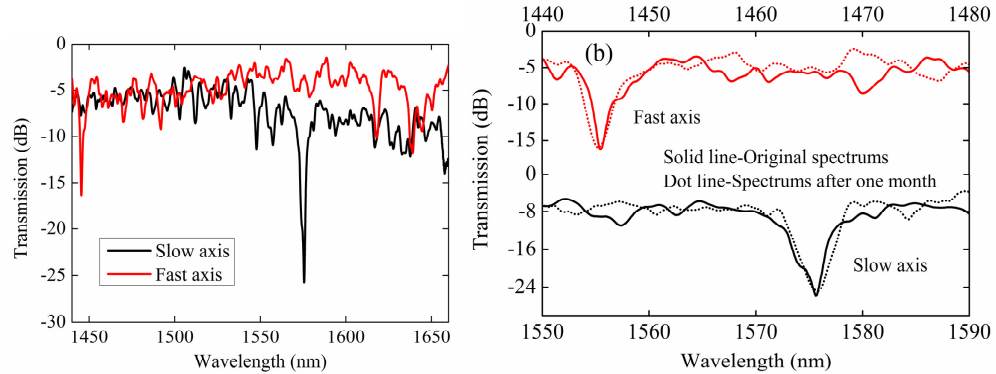


Fig. 11. (a) Transmission spectrums of an encapsulated Hi-Bi MF LPG. The LPG was inscribed on the non-encapsulated MF with a CO<sub>2</sub> laser before it is encapsulated. (b) The transmission spectrums of the LPG at different times (immediately after encapsulation and one month after encapsulation). The slow and fast axes correspond to the major and minor axes of the MF's elliptical cross-section.

## 5. Conclusion

We have demonstrated a simple, effective method for fabricating in-line photonic microcells (PMCs) with a tapered micro/nanometer-sized core encapsulated within a capillary tube. This microcell structure is proved to be robust, stable, not susceptible to contamination, and can be integrated into standard fiber optic systems, making MFs easier for some practical applications.

With an encapsulated Hi-Bi microfiber PMC spliced into a Sagnac loop interferometer, we demonstrated gas pressure and RI sensors with pressure sensitivity of 599 pm/bar and RI sensitivity of 2024 nm/RIU at  $\text{RI} \approx 1$ . With the same PMC, we also demonstrated liquid RI and temperature sensors and achieved RI sensitivity of 21231 nm/RIU at  $\text{RI} \approx 1.33$  and temperature sensitivity of  $-6.99 \text{ nm/}^{\circ}\text{C}$ . PMCs with encapsulated MF-based long period grating devices are also fabricated.

## Acknowledgments

This work was supported by the Hong Kong SAR Government through a GRF grant PolyU5177/10E, the Hong Kong Polytechnic University through a studentship, and the National Natural Science Foundation of China through Grant 61290313.